Analysis of Steam Explosions and its Consequences in Nordic BWR Cavity with MELCOR-TEXAS Coupling

Govatsa Acharya, Ibrahim Batayneh, Dmitry Grishchenko and Pavel Kudinov
KTH Royal Institute of Technology, Division of Nuclear Science and Engineering,
Albanova University Center, 10691 Stockholm, Sweden
govatsa@kth.se, batayneh@kth.se, dmitrygr@kth.se, pkudinov@kth.se

Abstract: Severe accident management in Nordic Boiling Water Reactors (BWRs) is achieved by quenching and cooling core debris ejected by the reactor vessel into a deep pool of water. However steam explosions can occur as a result of contact of hot corium particles with volatile coolant, challenging containment structures. Through a systematic ROAAM+ analysis it has been shown that the formation of coolable debris bed requires sufficiently deep pool of water in the cavity, which, unfortunately also significantly increases steam explosion loads. The present study focuses on analyzing steam explosions during severe accidents initiated by loss of coolant accident (LOCA) and station blackout (SBO) in Nordic BWRs using a framework based on dynamic coupling of MELCOR and TEXAS-V codes developed earlier. The analysis aims to assess if time evolution of the accident progression can limit possible conditions for the FCI and steam explosion, and then study the consequences in the cavity, particularly with concrete interactions and failure of the cavity basemat. The analysis of explosion impulse CDFs and failure probabilities obtained for selected transient analyses highlights that the non-reinforced hatch door has the highest failure probability with 95th percentile approaching 1 due to its low fragility limit of $6 kPa.s$, making failure likely in most scenarios. Mode of debris ejection seems to have a minor influence on the non-reinforced hatch door failure. Based on these unmitigated, conservative calculations, source term releases to the environment are large (at least two orders of magnitude above regulatory limits), with about half of the release as contaminated water. Results from these simulations enhance our understanding of the accident evolution on the steam explosion risks specific to Nordic BWRs and support improvements in accident management and containment design. The full model simulations will also be used in developing efficient and fast running dynamic surrogate models.

1. INTRODUCTION

Severe accident management (SAM) in Nordic boiling water reactors (BWRs) entails ejection and quenching of debris into a deep pool of water contained in the cavity (lower drywell (LDW)) beneath the reactor pressure vessel (RPV). This strategy presumes formation of a coolable debris bed that can maintain integrity of the containment (CNT) structures and reactor building components. Thus, large releases of radioactive fission products (FPs) to the environment (ENV) is avoided. While there is a need to verify the efficacy of the debris bed coolability, on the contrary, this SAM measure increases the risk of steam explosions (SE) as shown in earlier studies [6][7][8][9][10]. In the context of loss of containment integrity – specifically the failure of the containment wall/pedestal, or the cavity base/floor or the hatch door leading to the air-lock – a reasonable expectation is the loss of water inventory in the cavity and debris bed coolability. This certifies a loss of containment integrity and:

1. Opening of an unfiltered release pathway for FPs to the reactor building and the environment.
2. Uncovery of the debris bed, accelerating molten core concrete interaction (MCCI) leading to basemat failure and relocation of the corium to other parts of the reactor building.

In the case of ex-vessel SE that damages the containment structures, it behooves study of the timing of the CNT failure for appropriate assessment of the SAM measures. The dynamic evolution of the accident leading to and beyond the SE-induced failure is influenced by uncertainties in phenomena

(epistemic) and scenarios (aleatory). At KTH, the Risk-Oriented Accident Analysis Methodology+ (ROAAM+) is being developed to address and resolve such complex safety issues. ROAAM+ employs a combination of (i) detailed full models (FMs) and experiments necessary for obtaining information about key physics in different accident scenarios and (ii) computationally effective surrogate modes (SMs) that approximate FM solution, to enable comprehensive uncertainty, sensitivity and failure domain analysis [1][2][3][4][5].

In past studies [6][7][8][9], the effects of uncertainties in melt release conditions on SE risk and containment failure probabilities have been carried out. Fast running SM was developed to analyze uncertainties characterized by chaotic response to sensitive input parameters. The reinforcement of non-reinforced hatch door in the cavity was shown to drastically reduce the risk of containment failure for both oxidic and metallic melt release conditions. The radius of the melt jet, water pool depth and temperature of the melt were the most significant parameters [10] for the magnitude of SE in Nordic BWRs. The mode of debris ejection (either only molten debris or mixture of molten and solid debris) was shown to have a dominant effect on the containment loads. In these past ROAAM+ studies, the detailed mechanistic models have been represented with SMs that operated by non-time dependent variables. This simplified the SM model development process and helped in establishing links between different SMs. However, this was achieved at a loss of some potentially important information. Such simplifications were reasonably justified in the specific considered cases (melt release effects on SE and coolability).

In a general case, transient nature of the phenomena cannot be completely neglected or "effectively represented" with some averaged or "timeless" values. Examples of such cases where time is a non-negligible factor are scenarios with operator interventions (when outcome is dependent on the timing of event) and relatively slowly evolving containment phenomena (e.g. pool thermal-hydraulic behavior and fission product transport, deposition, re-entrainment and release). For this reason, to understand the impact of dynamic events, a coupling strategy between SE and severe accident system code was developed in [15]. While this preliminary study examined how the failure of a non-reinforced containment hatch door affects the subsequent release of FPs, its consequences on the debris bed interactions with basemat concrete was not studied. In the present paper, the same coupled framework is applied to a different FP pathway, one leading from the LDW to the environment, and simultaneously causing MCCI induced failure of the basemat. This work is expected to lead to expansion of the development of dynamic SM approaches to be used within the ROAAM+ framework.

2. APPROACH AND METHODOLOGY

2.1. Reactor Design

The plant under study is the 3900*MWth* Oskarshamn Unit 3, that is based on Westinghouse's BWR75 concept, as shown in Figure 2-1. The MELCOR model of the NBWR used in the study is the development of input deck originally created (v1.8.5) for the analysis of accidents in power uprated plants and maintained at KTH [14]. It has since then been updated to v2.2.18019 and currently for the analysis of the SA progression, v2.2.r2024 code is used [11][12] coupled together with TEXAS-V [13]. The containment itself is divided into control volumes (CVs) of the upper drywell (UDW) and lower drywell, wetwell (WW), blowdown pipes (BD pipes) and overflow pipes (OF pipes). The air-lock passageway at the base of the LDW provides access for maintenance and is protected by a hatch door. The height of this door is taken to be 3*m*. CV representing the rooms of the reactor building (RB) below the LDW (CV211) was added. In the O3 design, the pedestal supporting the RPV extends till the cavity floor and prevents corium reaching the WW [16][18]. The pedestal also leads to the air-lock, as well as secondary extensions. The supporting reactor systems are separated into four subsystems, and are housed beneath the cavity floor. From the schematics found in [17], a single CV for the entire cylindrical area encompassing the floor area of LDW and the annular WW, beneath the LDW is added. The outer diameter of the pedestal is about 12*m*, and the length of the air-lock is 6*m*, with the effective diameter

of CV211 being 27*m* (including width of the pedestal 1.8*m*) with a nominal height of 3.5*m*. The outer concrete wall is about 0.8*m* thick and the basemat floor itself is modelled to be 2*m* thick.

In addition to the inclined nature of the basemat (thicker at the centre), several cylindrical steel tube penetrations and a large drainage pipe going through the basemat exist. These penetrations can almost immediately fail upon contact with the hot debris bed, especially in dry cavity conditions. However in flooded conditions, with increased debris bed cooling, the interactions with penetrations need additional analysis. In order to protect these pipes and electrical penetrations, mechanical steel plates have been provided that physically prevent contact of the debris with the penetrations [20], as well as cooling channels [19] for better water circulation, local debris bed coolability and thermal protection. With SE and loss of water, coolability deteriorates and the penetrations fail. For this reason, a second CAV input for the reactor building (CV211) is included, with flowpaths from the damaged hatch door to RB via the air-lock itself (FL210) and basemat to the RB via basemat breach (FL215). FL210 is open when the hatch door fails, and a small fraction of water can accumulate in the RB*. Control functions control FL359 opening when CNT fails due to SE-induced failure of hatch door and FL215 opening when the basemat fails due to MCCI/penetrations failure. The FP release pathway is therefore assumed to be from the damaged LDW hatch door, eventually leading to the ENV – indicated as Pathway 2 in the figure.

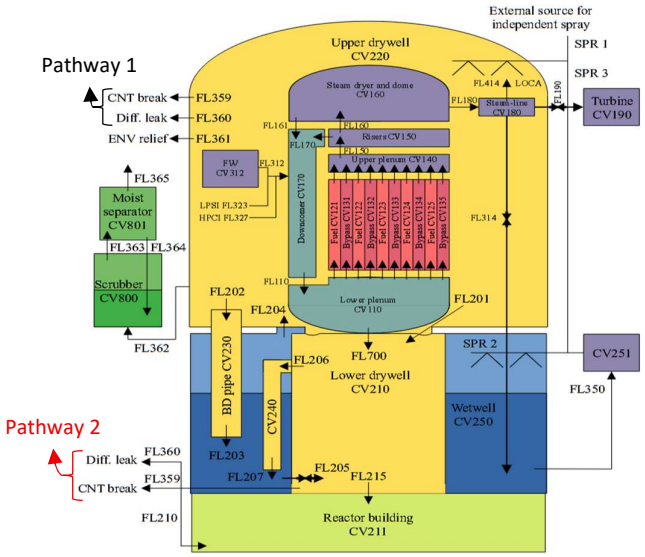

Figure 2-1 Schematic of the Nordic BWR. Pathway 1 was analyzed in [15].

In the input deck, standard CORCON-MOD3 model is employed for the coolant boiling curve enhancements, with constants (value = 1000) for oxidic and metallic debris conductivities and multiplier (value = 1000) on standard heat transfer on the bottom, side and interior surfaces [11][12]. RN pool scrubbing (IBUB) and water ingression models are turned off. Preliminary parametric study for the CV211 and corresponding heat structure dimensions (concrete walls and floor) was performed to establish a stable reference case that did not lead to crashed simulations. Results from a parametric study of debris bed spreading are presented in this paper.

2.2. Severe Accident Scenarios

Mainly two SA scenarios are studied here. These are classified for Nordic BWRs under release category 4 (RC4) – initiated by a transient or loss of coolant accident (LOCA), with containment failure due to containment phenomena. This release category has a significant contribution to unacceptable release frequency (URF) and large early release frequency (LERF). The first accident sequence RC4A is

* In reality, stairs lead from the air-lock level to the rooms beneath the cavity. It is assumed only a small fraction of water can flow through the hatch door break to RB, while most of it is being released/evaporated to the ENV.

initiated by large-break LOCA (LOCA) and the second sequence RC4B is initiated by station blackout (SBO). These two scenarios are split into two subcases based on the mode of debris ejection from the RPV [21]. ROAAM+ considers a phenomenological split for cases involving high epistemic uncertainties that cannot be resolved or bounded by standard analysis. The ejection mode is controlled by the IDEJ switch in MELCOR. With IDEJ0 (solid debris ejection ON), solid debris and molten debris can be ejected from the vessel and with IDEJ1 (solid debris ejection OFF), only molten debris can be ejected. The effect of limiting debris ejection to only molten materials is that the vessel wall is exposed to hot oxidic debris for a longer period, which results in accumulation of debris and delayed gross failure of the vessel LH wall. This affects the timing of the mass flow rates based on the selected filtering criteria, and thus the dynamic response. In total, four scenarios are considered, LOCA-IDEJ0, LOCA-IDEJ1, SBO-IDEJ0 and SBO-IDEJ1.

2.3. Dynamic Event Tree

Based on the dynamic coupling between MELCOR and TEXAS-V, for each of the 4 scenarios, initially a simulation is run not considering any SE, and ejection of debris upon RPV failure (no-CNT-failure). Based on the mass-averaged melt ejection rates, time instances when the rate exceeds the threshold for occurrence of SE (rate >50kg/s), are identified. A dynamic event tree (DET) set of these instances is prepared and MELCOR simulations are then successively run, assuming failure of the hatch door (opening of FL359 and FL210). In addition to the instances where rate >50kg/s, a case right when debris is ejected and collects on the cavity floor (coincidental with RPV failure) is included, assuming an early failure of the CNT basemat penetrations. The probability of FPs – cesium and iodine mass fractions of initial core inventory in particular – released to the ENV (conservatively including the FP fraction retained in the LDW pool lost through hatch door) is then combined with the probability of SE inducing the said CNT failure to derive cumulative distributions (CDFs) for release of FPs. As mentioned in [15], SEs occurring closest and farthest from the target yield two distinct CDFs, corresponding to highest and lowest SE impact load on the hatch door. For the propagation of the impulses, TNT method is applied.

3. RESULTS

Results from running MELCOR for 72h for all the 4 no-CNT-failure and reference SA scenarios, together with parametric study of debris bed spreading and dynamic SE MELCOR-TEXAS are presented in this section.

3.1. no-CNT-failure Category

Owing to the fact that CNT does not fail, CNT pressure increases rapidly during LOCA, and more gradually during SBO scenarios. The pressure evolution is presented in Figure 3-1. Consequently, in LOCA scenario, the CNT pressure sets off (at 5.5MPa) the filtered containment venting system (FCVS) via the multi-venturi scrubbing system (MVSS) even before RPV lowerhead failure (LHF). The opposite is true in the case of SBO. As a result, IDEJ does not influence TFCVS during LOCA, while it delays TFCVS in SBO-IDEJ1 compared to SBO-IDEJ0 – a quicker ejection of hot solid+molten debris mass to the cavity (IDEJ0) causes rapid evaporation of water and CNT pressurization compared to a delayed molten debris ejection (IDEJ1), that are shown in Figure 3-2.

Except for the case of LOCA-IDEJ1, almost 300$tons$ of debris is ejected to the cavity. As seen from the masses of degraded core materials in Figure 3-3, in LOCA-IDE1 a higher portion of solid particulate debris is held back in the lower plenum (LP) together with molten materials, compared to all other cases. This has direct bearing on the mass flow rates of the debris once lowerhead (LH) of the RPV fails, with rates of ejection of ZrO2 and UO2 defined by the melt fraction (of Zircaloy) available in the lowest segment of LH [11][12]. It can be observed that for IDEJ0 cases, irrespective of SA scenario, negligible debris masses remain in the RPV, while non-negligible masses remain in case of IDEJ1. This leads to divergence of accident progression post-LHF for LOCA and SBO, as witnessed in the timing of key events shown in Table I.

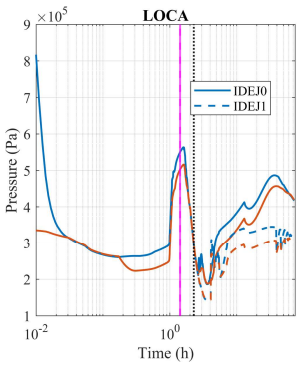

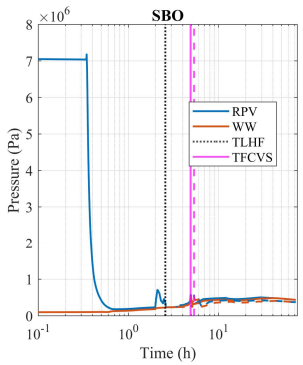

Figure 3-1 Pressure in the CNT and WW for the 4 SA scenarios. Solid lines indicate IDEJ0 cases and dashed lines indicate IDEJ1 cases. TLHF: time of RPV lowerhead failure, TFCVS: time of FCVS activation.

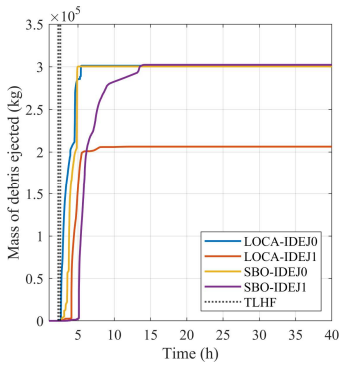

Figure 3-2 Mass of debris ejected to the cavity. Earlier TLHF corresponds to LOCA.

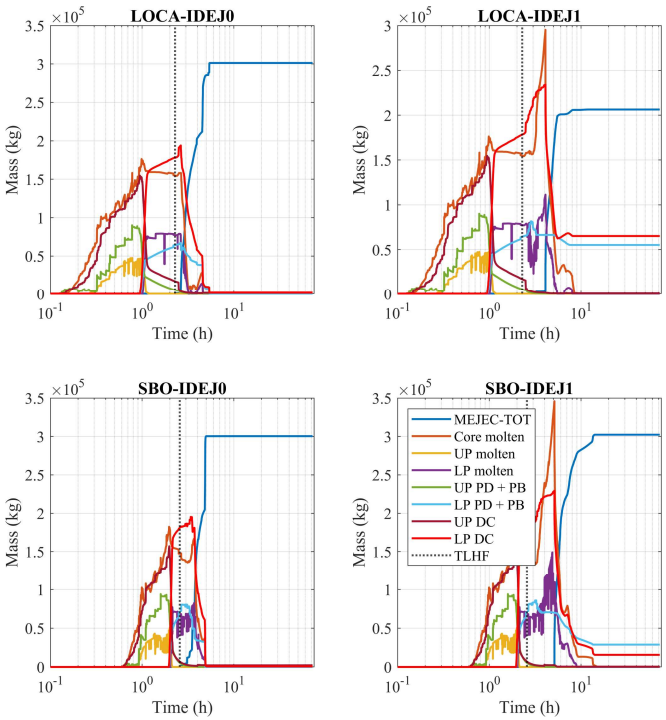

Figure 3-3 Mass of molten pool and debris in the vessel for 4 SA scenarios. UP molten and LP molten: molten mass in the core and lower plenum regions, PD: particulate debris, PB: particulate debris in the bypass channel, DC: conglomerate debris.

The v18019 details shown for comparison of the similar no-CNT-failure SA cases are drawn from [21]. While no differences between r2024 and 18019 are observed until commencement of fuel element melting, core degradation and heat transfer in oxidation model could influence and vary contact areas, contact times and temperature of reactants. The addition of CVs and HSs in r2024 input deck, while leads to quicker relocation of debris to the LP in LOCA and SBO, results in delayed LHF in LOCA and early LHF in SBO – all compared to v18019 without any additional CV for reactor building. Another observation in the ex-vessel phase of no-CNT-failure category simulations is that, despite FCVS pressure relief, due to excessive superheated steam bubbling in MVSS during LOCA-IDEJ1 scenario, the scrubber essentially dries out, resulting in release of FPs to the ENV after ~62h. Additionally, activation of automatic depressurization system (ADS) from the RPV steam lines during SBO, directly

into the WW increases WW water temperatures that by ~66*h*, WW pool starts to boil – a consequence being late release of FPs retained/scrubbed within the WW pool if CNT were to fail.

Table I: Timing [*s*] of key events during 4 no-CNT-failure scenarios. Details of v18019 from [21].

Key event	LOCA-IDEJ0		LOCA-IDEJ1		SBO-IDEJ0		SBO-IDEJ1	
	r2024	v18019	r2024	v18019	r2024	v18019	r2024	v18019
L4 (0.5*m* above TAF)	9	9	9	9	7	7	7	7
Core uncovery	9	9	9	9	838	838	838	838
L6 (1*m* below TAF)	27	27	27	27	1111	1111	1111	1111
ADS ON	-	-	-	-	1235	1235	1235	1235
Gap release	220	220	220	220	2008	2008	2008	2008
Particulate debris formation	477	477	477	477	2229	2236	2229	2236
Cavity flood	625	625	625	625	1950	1950	1950	1950
Fuel element degradation	866	866	866	866	2916	2916	2916	2916
Relocation to lowerhead	3302	4606	3302	4606	6938	7238	6938	7238
RPV failure	8205	6246	8205	6246	9235	9841	9235	9841
MVSS vent	5130	5130	5130	5130	17602	20280	19250	25920
MEJEC >70*tons*	10240	9529	15058	17825	13432	10978	18741	20034
LDW at saturation	14155	12510	20280	18859	16418	14340	23618	25555
WW at saturation	-	-	-	-	253218	-	241612	243159
MVSS dryout	-	-	222194	220972	-	-	-	-

The mass-averaged mass flow rates calculated considering mass ejected for every 5*s* or 100*s* period are shown in Figure 3-4(a) and (b). The corresponding time instances when flow rate exceeds the filter threshold is presented in Figure 3-5. As seen, specifically for IDEJ0 scenarios, ejection rate is large subsequent to LHF (~3*h*). There is a second burst of large mass ejection at ~4.5-5*h*. For IDEJ1 scenarios, no large ejection is observed immediately after LHF. Only once solid debris melts and is available in cells adjacent to LH, does the flow rate picks up (after ~4*h*). However, the number of such filtered time instances is less compared to IDEJ0 scenarios – calculated to be 26, 6, 34 and 13 for LOCA-IDEJ0, LOCA-IDEJ1, SBO-IDEJ0 and SBO-IDEJ1 respectively. In addition, CNT is also assumed to fail coincidental with LHF failure – SE and failure of basemat penetrations on contact with corium.

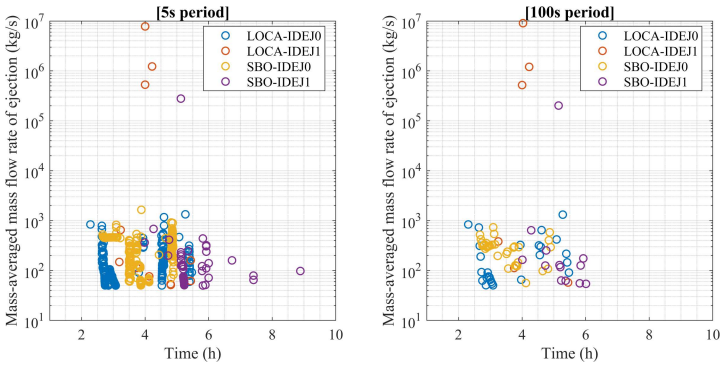

(a) (b)

Figure 3-4 Mass-averaged mass flow rates for (a) 5*s* and (b) 100*s* period. Instances presented after filtering (>50*kg/s*).

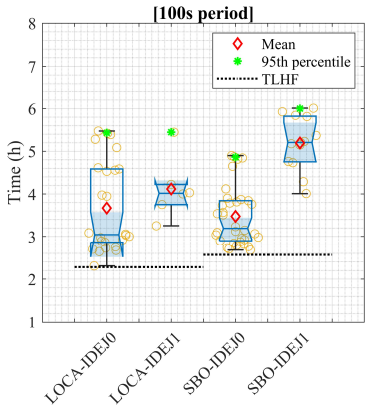

Figure 3-5 Time instances after filtering for flow rates >50*kg/s*.

3.2. Reference CNT Failure Cases and Preliminary Parametric Study of Debris Spreading

In the reference case, SE is assumed to cause hatch door failure exactly when LH fails and first ejected debris contacts cavity pool. This leads to rapid loss of coolant from LDW as well as WW that

replenishes the cavity. As presented in Table II, for LOCA scenario LDW is completely dry within 39560-41860s, and for SBO within 20430-28140. The corium configuration in the cavity during LOCA-IDEJ0 is mainly as HMX (mixed phase, more dense than metallic phase) in the early ex-vessel phase and LOX (pure oxide phase, less dense than metallic phase) in the late ex-vessel phase (post-LDW failure). During LOCA-IDEJ1, the composition is LMX (mixed phase, less dense than metallic phase) in the early ex-vessel phase and LOX in the late ex-vessel phase. Whereas in SBO it is HMX in the early ex-vessel phase and LOX in the late ex-vessel phase.

Table II: Timing [s] of key events during 4 reference CNT-failure scenarios (r2024).

Key event	LOCA-IDEJ0	LOCA-IDEJ1	SBO-IDEJ0	SBO-IDEJ1
LDW dryout	39560	41860	20430	28140
MCCI commencement	59601	64400	14820	18130
LDW failure	191402	218000	177600	227000

MCCI attack on the basemat leads to the generation of non-condensable and combustible gases. The time evolution of generation of H2, CO, CO2 and H2O in the two CAVs, as well as H2 generated as a result of oxidation in the core are presented in Figure 3-6. A direct consequence is the increase in pressure of the containment as well as increased transfer of FPs carried by steam to the ENV. It is observed that rate of production of CO is initially high (commencing at ~14630-19450s for all 4 SA scenarios), and plateaus within about ~100000s. In IDEJ1 scenarios, CO is the single largest gas produced by mass, whereas in IDEJ0 scenarios CO is initially the largest, and later surpassed by CO2. In IDEJ0 cases, marginally significant amounts of H2O is also generated. It is also observed that H2 generated as a consequence of MCCI is larger than H2 generated by oxidation in the core structures.

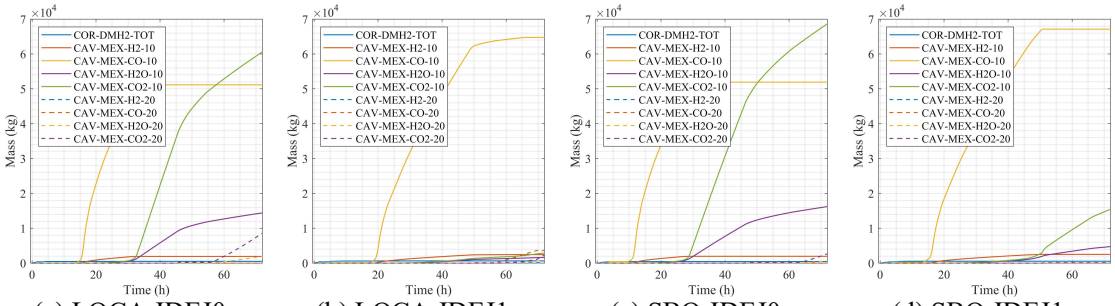

(a) LOCA-IDEJ0. (b) LOCA-IDEJ1. (c) SBO-IDEJ0. (d) SBO-IDEJ1.

Figure 3-6 Mass of gases produced by MCCI reactions in the cavity basemat and oxidative hydrogen in the core for 4 SA scenarios. LDW is CAV_10 and RB is CAV_20.

By default, MELCOR makes an assumption that all the debris in the cavity is spread instantaneously and evenly throughout the floor. It is also possible to enable internal debris spreading model – based on two phase viscosity enhancements with either Kunitz correlation (default) or Ramacciotti correlation [11][12]. As for the radius of the debris bed MELCOR offers (i) user defined radius (with control functions), (ii) internally calculated radius, (iii) RPV breach area as the initial radius or (iv) zero as the initial radius. In BWRs typically the failure of the RPV occurs in the LH penetrations, with multiple jets, or in case of plugged penetrations a gross failure may occur with a large breach area, and the ejected corium effectively covers the entire basemat area. A concise parametric study is performed by activating the default internal debris spreading model and varying the maximum debris bed radius to be {2.03, 3.05, 4.06, 5.08, 6.1}m, with the last radius being the radius of the reference case. The time of LDW failure for the considered cases is presented in Table III. The time of beginning of debris ejection to the cavity for all cases is same as time of RPV failure in Table I.

However, it is seen that with a very small debris bed radius (2.03m, narrow tall cylindrical shape), the rate of MCCI ablation of concrete basemat is exceedingly quick, such that even before complete LDW dryout, the basemat failure occurs within ~24855-38525s. With increasing radius, the time of LDWF also increases. Despite variations in the time of LDWF, the final release of FPs to the ENV, as well as

hydrogen generation by MCCI reactions, were observed to be about the same. A larger parametric study is in progress with additional uncertain MCCI parameters, and the results would be presented In the future.

Table III: Timing [s] of LDW failure for varying debris bed radius.

Maximum radius [m]	LOCA-IDEJ0	LOCA-IDEJ1	SBO-IDEJ0	SBO-IDEJ1
2.03	24855	32774	35524	38525
3.05	65640	67229	51736	74407
4.06	95587	113904	66011	100952
5.08	97342	160312	78628	115470
6.01	191402	218000	177600	227000

3.3. TEXAS-V Calculations of Steam Explosion Impulse Loads

DET simulations for MELCOR assuming failure of the hatch door, and TEXAS-V premixing simulations considering thermal-hydraulic conditions of the cavity pool and ejected melt jet at the time instances mentioned earlier are run. For the SE, the triggering time is a cause for uncertainty in the explosion impulses [7]. To alleviate this issue and make the model well-posed, statistical distributions of the impulses at the exact premixing conditions but varying triggering time is considered. The explosion impulses distribution is then utilized for the derivation of the probability of exceeding the fragility limits of failure of the target structures.

For the non-reinforced hatch door, a $6kPa.s$ fragility limit of failure is considered [7]. The propagation of SE impulses on to the hatch door in the near and far conditions for each dynamic branching (colour coded based on time instances) are presented in Figure 3-7. LOCA-IDEJ1 has some of the largest impulses even in the case when SE occurs farther from the hatch door. This is followed by SBO-IDEJ1 scenario. This is corroborated by the fact that for a few instances, see Figure 3-4(b), a large amount of debris is ejected to the cavity (>100$tons/s$) resulting in high impulse magnitudes, even when SE is far.

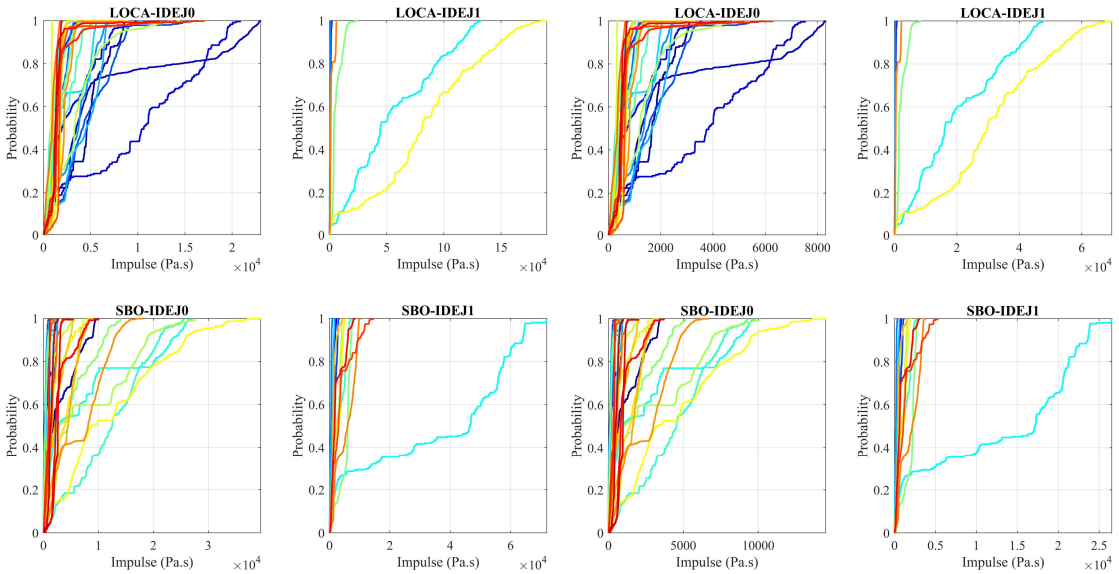

(a) SE near. (b) SE far.

Figure 3-7 eCDFs of impulses on the hatch door considering SE point source (a) near the hatch door and (b) at the top of water pool for 4 SA scenarios. Colour indicates the time instance of SE premixing: blue is early, red is late.

For the IDEJ0 scenarios, more instances of SE premixing cases lead to exceedance of the fragility. The corresponding probabilities of failure of the hatch door are provided in Figure 3-8 and Figure 3-9. For the IDE0 cases, ~85-90% of lower bound instances remain “safe” (does not exceed the fragility) while ~55-75% of upper bound instances cause failure. For the LOCA scenario, typically early SE have higher probability of failing the hatch door, as compared to SBO, where mid- late instances can lead to failure.

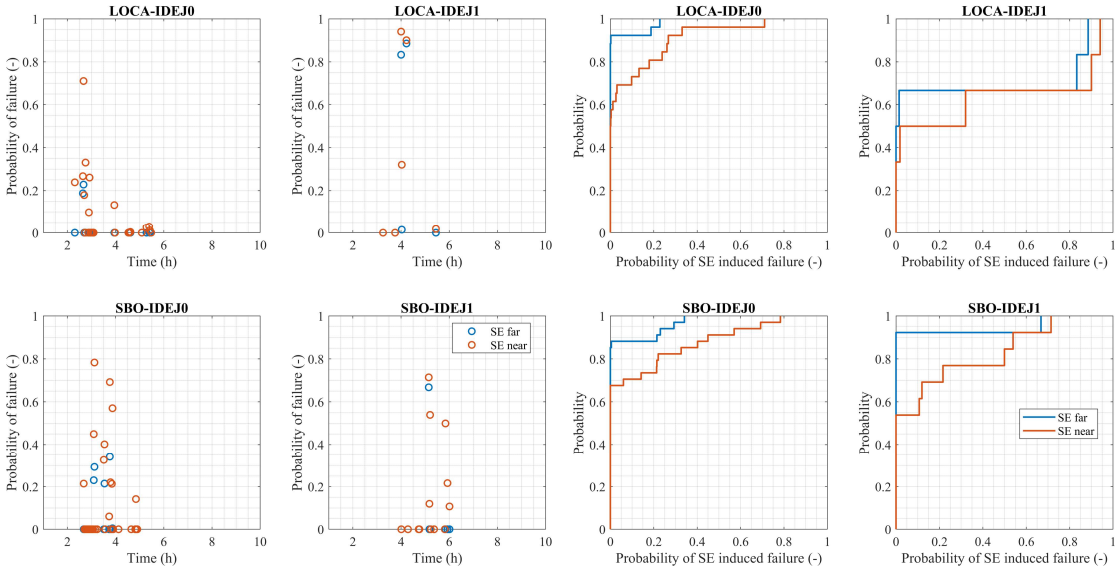

Figure 3-8 Probabilities of failure for the non-reinforced hatch door.

Figure 3-9 Empirical CDFs of failure probabilities for the non-reinforced hatch door.

3.4. Reactor Conditions in Dynamical Cases of Steam Explosions

The pressure evolution in the containment UDW and the amount of debris ejected from the RPV to the cavity for DET cases are presented in Figure 3-10. The individual branching from the initial no-CNT-failure case are observed. The effect of CNT pressure relief (by SE-induced failure of CNT) on debris ejection variability is higher in the case of IDEJ1 than IDEJ0 – potential for secondary SEs is higher.

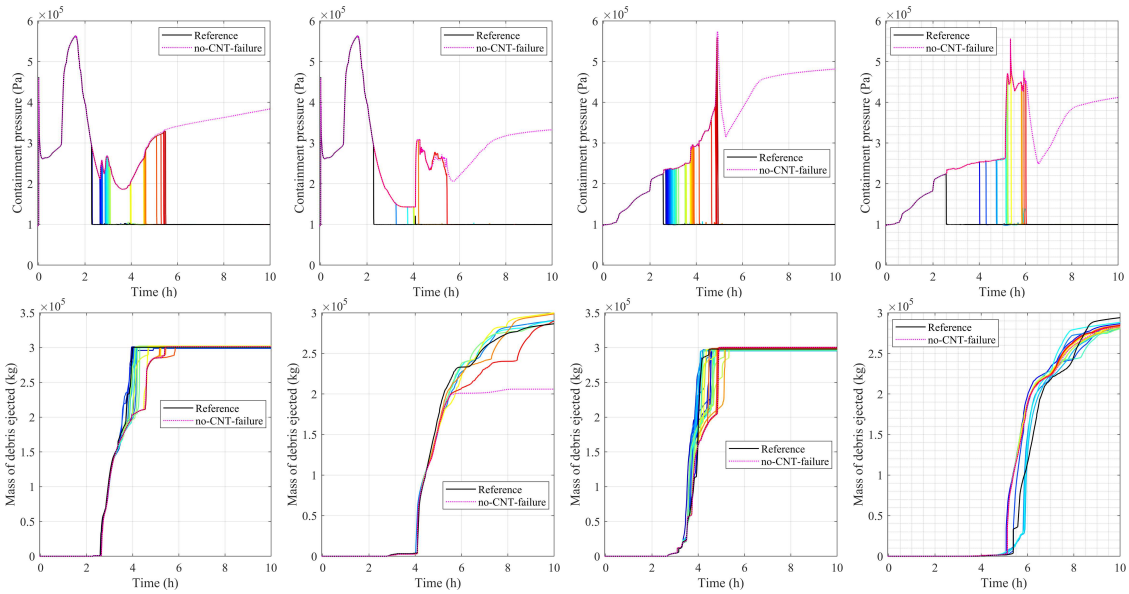

(a) LOCA-IDEJ0. (b) LOCA-IDEJ1. (c) SBO-IDEJ0. (d) SBO-IDEJ1.

Figure 3-10 CNT pressure (top) and mass of debris ejected (bottom) for 4 SA scenarios.

In all the scenarios, pressure that reduces as a result of containment venting, gradually increases as LDW evaporates faster, until eventual failure of the CNT by SE. The timing of key events for the cases in DET set are presented in Figure 3-11. In the LOCA scenario, effect of IDEJ on MCCI is very evident in the fact that time of MCCI commencement has larger range in IDEJ1 than in IDEJ0. The same holds

true for SBO scenario. In IDEJ1, the already molten debris ejected to the cavity, almost immediately reacts with the basemat concrete to release gaseous products. Time of large (>70*tons*) debris ejection in IDEJ1 is delayed by about an hour compared to IDEJ0, which itself is delayed by about another hour from LHF. This delay is propagated to succeeding ex-vessel phenomena such as WW and LDW pool boiling and LDW failure. In most of the cases considered, the LDW fails by 72*h* due to MCCI ablation.

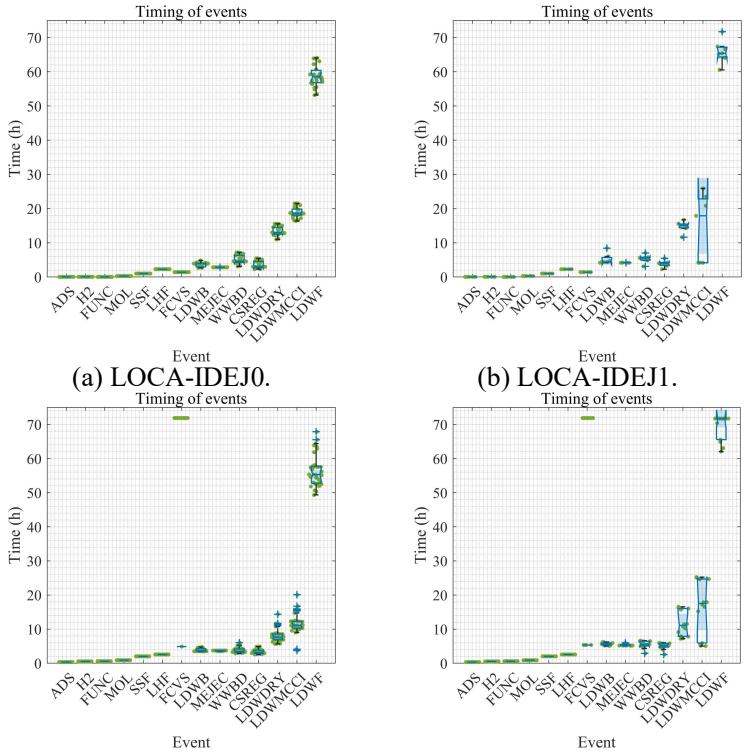

(a) LOCA-IDEJ0. (b) LOCA-IDEJ1.

(c) SBO-IDEJ0. (d) SBO-IDEJ1.

ADS: time of ADS activation, H2: time of hydrogen generation/gap release, FUNC: time of full core uncovery, MOL: time of fuel degradation and molten debris formation, SSF: time of failure of support plate, FCVS: time of FCVS activation (t=72*h* if no activation), LDWB: time of LDW pool boiling, MEJEC: time of large debris mass ejection (>70*tons*), WWBD: time of WW pool boiling, CSREG: time of cesium release mass fraction > 0.001, LDWDRY: time of LDW dryout, LDWMCCI: time of commencement of MCCI, LDWF: time of failure of LDW.

Figure 3-11 Timing distributions of key events for the dynamic branching cases of 4 SA scenarios.

3.5. Source Term Empirical CDFs

The mass fractions of cesium (RN class 2: CsOH, class 16: CsI and class 17: CsM) and iodine (RN class 4: I2 and class 16: CsI) are extracted for all the dynamic cases. The empirical CDF for the final mass fraction released to the ENV (both in atmosphere phase and pool phase) is determined and as described in [15] the step values of the CDFs are updated with the probabilities calculated from TEXAS-V for near and far SEs. The updated eCDFs for the final source term releases are presented in Figure 3-12.

Several differences with the pathway 1 results [15] can be seen. In pathway 2, in addition to atmospheric release of FPs, retained FPs in pool is also lost, the source term release is much higher – in the case of Cs it exceeds the regulatory limits by at least 2 orders of magnitude (0.1% of initial inventory). In the case of LOCA Cs mass fraction of about 0.25-0.3 is released while I2 mass fraction of around 0.45-0.5 is released. Whereas for SBO, about ~0.5 and ~0.7 of Cs and I2 mass fractions respectively are released. The uncertainty in the release fractions in case of SBO is smaller. The higher probabilities of SE-induced failure for LOCA-IDEJ0 (at 2.5*h* in Figure 3-8) and LOCA-IDEJ1 (at 4*h* in Figure 3-8) correspond to the abrupt jumps in the updated CDFs. For SBO-IDEJ0 (except for three cases with high probability for SE far) and SBO-IDEJ1 (except for one case with high probability for SE far), updated CDFs follow original CDFs. For iodine, probability of large releases occurring is higher in all scenarios except for SBO-IDEJ0. Given that LOCA-IDEJ1 and SBO-IDEJ1 with just 6 and 13 cases each, may not be statistically represented, and thus the filtered 5*s* period data instead of the 100*s* considered in this study would yield more reasonable results.

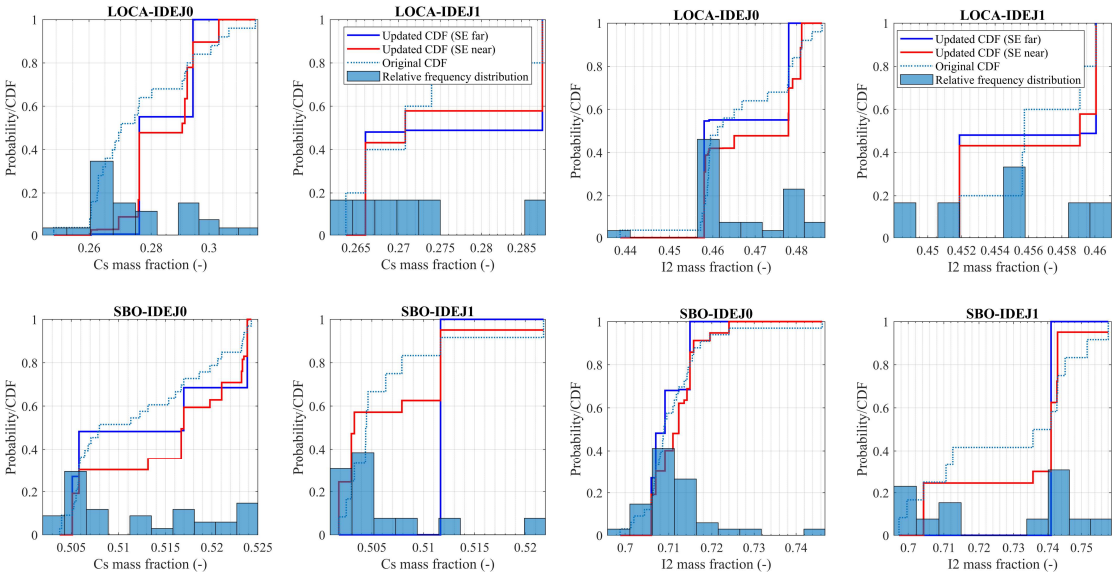

(a) Cs mass fraction. (b) I2 mass fraction.

Figure 3-12 eCDFs of final FP release fractions for 4 SA scenarios.

4. CONCLUSIONS

In this study, the dynamic coupling between MELCOR (v2.2.2024) and TEXAS-V developed earlier is expanded to include additional FP release pathways and MCCI in the cavity of Nordic BWRs. Broadly two different scenarios (with 2 splinters each) are studied. The cases without any SE-induced CNT failure is described and relevant debris ejection conditions are described to create a branching set for a DET. Cases involving IDEJ0 result in statistically larger and early instances of potential SE occurrence. Pathway 2 explored here is dynamically more challenging as the CNT failure leads to cavity dryout and MCCI led basemat failure. The timing of the key events were characterized. For SBO reference scenarios, it is observed that MCCI commences even before LDW has dried out completely. However, considering DET branching, it is seen that irrespective of LOCA or SBO, it is IDEJ that increases uncertainty in the timing of MCCI in the LDW (specifically for IDEJ1). The uncertainty introduced by timing of MCCI commencement does not translate to uncertainty in timing of LDW failure. In addition, combined with early LDW dryout, basemat meltthrough is seen to occur earlier in IDEJ0 than in IDEJ1.

The reference MELCOR model used here is based on preliminary parametric study performed by varying debris bed sizes and switching between internal debris spreading models. The cavity definition for the reactor building CV modifications, have shown peculiarities in radial and axial ablation rates – sometimes even unphysical radial failure of vertical pedestal walls preceding axial failure of basemat floor. In the future these discrepancies would be corrected and a thorough parametric and sensitivity studies will be performed for pathway 2 configuration.

Acknowledgements

This work is supported by the Nordic Nuclear Safety Research (NKS), under the NKS-R STATUS activity (Contract: AFT/NKS-R(21)133/5) and by the SSM ROAAM+ project at the KTH, Sweden.

References

1. P. Kudinov, et al., “A Framework for Assessment of Severe Accident Management Effectiveness in Nordic BWR Plants”, *12th Probabilistic Safety Assessment and Management (PSAM12)*, Honolulu, Hawaii, June 22–27 (2014).

2. W. Villanueva, et al., "Coupled thermo-mechanical creep analysis for boiling water reactor pressure vessel lower head", *Nuclear Engineering and Design*, **249**, pp. 146-153 (2012).
3. C.T. Tran, et al., "An approach to numerical simulation and analysis of molten corium coolability in a BWR lower head", *Nuclear Engineering and Design*, **240**, pp. 2148–2159 (2010).
4. S.E. Yakush, P. Kudinov, "In-vessel debris bed coolability and implications for vessel failure mode", *11th International Topical Meeting on Nuclear Reactor Thermal Hydraulics Operation and Safety (NUTHOS11)*, Gyeongju, Korea, October 9-13, N11P0532 (2016).
5. V.-A. Phung, et al., "Prediction of In-Vessel Debris Bed Properties in BWR Severe Accident Scenarios using MELCOR and Neural Networks", *Annals of Nuclear Energy*, **120**, pp. 461-476 (2018).
6. D. Grishchenko, et al., "Failure domain analysis and uncertainty quantification using surrogate models for steam explosion in a Nordic type BWR", *Nuclear Engineering and Design*, **343**, pp. 63-75 (2019).
7. D. Grishchenko, et al., "Development of a surrogate model for analysis of ex-vessel steam explosion in Nordic type BWRs", *Nuclear Engineering and Design*, **310**, pp. 311-327 (2016).
8. D. Grishchenko, P. Kudinov, "Validation of a Full Model for the Analysis of Ex-Vessel Steam Explosion in LWRs", *18th International Topical Meeting on Nuclear Reactor Thermal Hydraulics (NURETH18)*, Portland, OR, August 18-23 (2019).
9. D. Grishchenko, et al., "Risk of containment failure due to ex-vessel steam explosion for Nordic BWRs", *18th International Topical Meeting on Nuclear Reactor Thermal Hydraulics (NURETH18)*, Portland, OR, August 18-23 (2019).
10. S. Galushin, et al., "Analysis of the Effect of Vessel Failure and Melt Release on Risk of Containment Failure Due to Ex-Vessel Steam Explosion in Nordic Boiling Water Reactor Using ROAAM1 Framework", *Nuclear Engineering and Radiation Science*, **6**(4), pp. 041113 (2020).
11. L.L. Humphries, et al., *MELCOR Computer Code Manuals Vol. 1: Primer and Users' Guide Version 2.2 r2023*, SAND2023-10997 O, Sandia National Laboratories, Albuquerque, NM (2023).
12. L.L. Humphries, et al., *MELCOR Computer Code Manuals Vol. 2: Reference Manual Version 2.2 r2023*, SAND2023-10994 O, Sandia National Laboratories, Albuquerque, NM (2023).
13. M.L. Corradini, et al., "Users' manual for Texas-V: One dimensional transient fluid model for fuel-coolant interaction analysis", University of Wisconsin-Madison, Madison, WI (2002).
14. L. Nilsson, *Development of an Input Model to MELCOR 1.8.5 for Oskarshamn 3 BWR*, SKI Report 2007:05 (2006).
15. G. Acharya, et al., "Analyzing steam explosions during severe accidents in Nordic BWRs with MELCOR-TEXAS coupling", *Nuclear Engineering and Technology* (2026), https://doi.org/10.1016/j.net.2026.104312.
16. T. Okkonen, et al., *Quantification of the Ex-vessel Severe Accident Risks for the Swedish Boiling Water Reactors: A Scoping Study Performed for the APRI Project*, SKI Report 95:76 (1995).
17. S. Hirschberg, L.I. Tirén, *Design-Related Defensive Measures Against Dependent Failures. ABB ATOM's Approach*, In: Amendola, A. (eds) Advanced Seminar on Common Cause Failure Analysis in Probabilistic Safety Assessment. ISPRA Courses on Reliability and Risk Analysis, vol 5. Springer, Dordrecht (1989).
18. K. Becker, *RAMA III Final report*, RAMA-85/4, January, S-611 82, Studsvik Library, Nyköping, Sweden (1985).
19. W. Frid, CONTAINMENT SEVERE ACCIDENT THERMOHYDRAULIC PHENOMENA, *RAMA III Final report*, RAMA-89/4, August, 611 82, Studsvik Library, Nyköping, Sweden (1989).
20. STATENS KÄRNKRAFTINSPEKTION, *2003 Störningshandboken BWR*, SKI Rapport 03:02, ISSN: 1104-1374 (2003).
21. G. Acharya, et al., "Effect of Debris Ejection Mode on the Accident Progression and Source Term in Nordic BWRs", *32nd International Conference on Nuclear Engineering (ICONE32)*, June 22-26, China (2025).